Electrocatalysis
https://doi.org/10.1007/s12678-022-00742-6

ORIGINAL RESEARCH

Transition Metal Atoms Anchored on $CuPS_3$ Monolayer for Enhancing Catalytic Performance of Hydrogen Evolution Reactions

Yongxiu Sun[1] · Aijian Huang[1,2] · Zhijie Li[1] · Yong-Qing Fu[3] · Zhiguo Wang[1]

Accepted: 22 April 2022

Abstract

The noble metal such as Pt has been used as the catalysts for hydrogen evolution reaction (HER), but with problems such as scarcity of resources and high cost. Anchoring transition metal atoms onto the catalysts is regarded as a potential approach to solve this problem and enhance the electrocatalytic performance of HER. For this purpose, two-dimensional materials, such as $CuPS_3$ monolayer, are regarded as one of the most ideal carriers for adsorption of metal atoms. However, there is no previous study on this topic. In this paper, we systematically studied microstructures, electronic properties, and electrocatalytic performance of the $CuPS_3$ monolayer anchored with transition metal atoms (e.g., Sc, Ti, V, Cr, Mn, Fe, Co, and Ni) using a density functional theory (DFT). Results showed that all the transition metal atoms are favorably adsorbed onto the $CuPS_3$ monolayer with large binding energies at the top of the Cu atom. The pristine $CuPS_3$ monolayer has a large catalytic inertia for hydrogen evolution reactions, whereas after anchored with transition metal atoms, their catalytic performances have been significantly improved. The Gibbs free energy (ΔG_H) is 0.44 eV for the H atom absorbed onto the pristine $CuPS_3$ monolayer, whereas the ΔG_H values for the V, Fe, and Ni atoms anchored onto the $CuPS_3$ monolayer are 0.02, 0.11, and 0.09 eV, respectively, which is close to the ΔG_H of H atom adsorbed on Pt (e.g., −0.09 eV). At the same time, the influence of hydrogen coverage rate was calculated. The result shows that V adsorbed on $CuPS_3$ monolayer is catalytic active for HER for a large range of hydrogen coverage. Our results demonstrate that anchoring of V atom onto the $CuPS_3$ monolayer is a potentially superior method for making the catalyst for the HER.

Keywords $CuPS_3$ monolayer · Transition metal atom · Hydrogen evolution reaction · Density functional theory

Introduction

There are increasing concerns about the global environmental pollution, which results in a strong demand for the alternative green energy sources to replace the traditional fossil fuels [1]. As one of the promising and sustainable energy sources, hydrogen energy generated from electrocatalytic water splitting is attractive because of its simple reduction process of H_2O, without much pollution generated [2]. Noble metal Pt-based catalysts have shown effective stabilities for the production of H_2 from water through hydrogen evolution reaction (HER) [3]. However, their high cost and scarcity significantly hamper the practical applications, and thus it is critical to develop low cost and earth-abundant catalyst materials with an extraordinary electrocatalytic performance [4]. In recent years, a number of advanced non-noble catalysts for HER have been studied, such as nickel molybdenum alloys [5] dichalcogenides [6], carbides [7], nitrides [8], phosphides [9], and phosphosulfides [8].

In addition to the excellent catalytic activity, the maximum utilization of metal atoms has also been studied for HER [10, 11]. Therefore, single-atom catalysts (SACs) have received extensive attention [12]. Based on references [13], individually separated atoms can improve the catalytic activity and selectivity of electrochemical reaction. However, because the high surface–free energy makes these single atoms easily aggregated during the catalytic process. Thus,

✉ Yong-Qing Fu
Richard.fu@northumbria.ac.uk

✉ Zhiguo Wang
zgwang@uestc.edu.cn

[1] University of Electronic Science and Technology of China, Chengdu 610054, People's Republic of China

[2] Department of Chemistry, Tsinghua University, Beijing 100084, China

[3] Faculty of Engineering and Environment, Northumbria University, Newcastle Upon Tyne NE1 8ST, UK

Published online: 03 May 2022

single atoms should be anchored on a suitable substrate to establish a stable platform [14], which could increase atom utilization caused by the high dispersion of individual atoms [15]. As the isolated and individual metal atoms adsorbed on the substrates, the increase of catalytic active sites, the increase of unsaturated coordination number of metal atoms and the interaction between single metal atom and the substrates can lower the energy barriers of electrochemical reactions and improve the electrocatalytic activity for HER [16]. Up to now, transition- metal atoms–based SACs are the hot research topic in the field of electrocatalyst for HER, such as Fe adsorbed on graphdiyne [17], Mo adsorbed on silicene [18], transition metal atoms adsorbed on transition metal dichalcogenides [19, 20], and Co–Ni adsorbed on nitrogen-doped graphene [21–23].

Due to their large specific surface area and high carrier mobility, two-dimensional materials have become a good support material for SACs in recent years, such as graphene [24], silicene [25], metal sulfides[26], and metals oxides[27]. Among all two-dimensional materials, ternary metal thiophosphates as the supports for the SACs was rarely studied. Recently, Xiao et al. prepared Ni atom anchored onto $FePS_3$ nanosheets which enhanced water adsorption and dissociation process, thus accelerating the HER [28]. Strong interactions between Ni atom and $FePS_3$ nanosheets can tune the electronic structures of $FePS_3$ nanosheets. Hence, the catalytic activity of HER for $FePS_3$ was improved [28]. Until now, the $CuPS_3$ monolayer as the support for the adsorption of transition metal atoms has not been reported. As a member of the family of ternary metal thiophosphates, $CuPS_3$ has similar electrochemical properties compared to those of $FePS_3$ and can be considered as a support material for transition metal atoms. $CuPS_3$ monolayer is composed of Cu and P atoms in an octagonal structure of S atoms, and have Cu and P atoms between two sheets of S atoms [29]. This structure provides a large specific surface area and many adsorption sites for transition metal atoms to be anchored and thus achieves a good thermodynamic stability [30]. $CuPS_3$ monolayer can be easily obtained by exfoliating their bulk counterpart into a layered structure due to the van der Waals (vdW) interactions between each layers, which opens up the possibility of mass productions [31]. Inspired by the above, it is critical to adjust the surface catalytic site and electronic structure of $CuPS_3$ monolayer to enhance its catalytic activity for HER.

Herein, the structures, electronic properties and electrocatalytic performance of a $CuPS_3$ monolayer anchored with transition metal atoms (e.g., Sc, Ti, V, Cr, Mn, Fe, Co, and Ni) were investigated using a density functional theory (DFT). Results showed that all the transition metal atoms are favorably adsorbed onto the $CuPS_3$ monolayer with large binding energies. The pristine $CuPS_3$ monolayer has a large catalytic inertia for HER, whereas their catalytic performance has been significantly improved after anchored with transition metal atoms. Among them, the adsorption Gibbs free energies (ΔG_H) for the V, Fe, and Ni atoms anchored onto the $CuPS_3$ monolayer are 0.02, 0.11, and 0.09 eV, respectively. The values of the ΔG_H are comparable to precious metal catalyst [32]. At the same time, the influence of hydrogen coverage rate was calculated. The result shows that V adsorbed on $CuPS_3$ monolayer is catalytic active for HER for a large range of hydrogen coverage. Our results suggest that anchoring of V atom on $CuPS_3$ monolayer represents a new generation of catalyst for hydrogen evolution reaction.

Computational Details

All the DFT calculations were performed with the SIESTA code [33], using the generalized gradient approximation with the scheme of Perdew-Burke-Ernzerhof (GGA-PBE) functional [34]. Norm-conserving pseudopotentials were used to describe the electron–ion interactions, and double-ζ basis sets with the polarization function (DZP) were used to describe the valence electron wave functions [33]. The conjugate gradient (CG) method was used for the structural optimizations, and the Brillouin zone was sampled by $15 \times 15 \times 1$ k-point mesh within the Monkhorst–Pack(MP) scheme [35]. The atomic positions and lattice parameters were fully relaxed until the force on each atom was less than 0.01 eV/Å. A vacuum of thickness 30 Å was added perpendicular to the surface of monolayer to avoid any spurious periodic interactions.

Under the standard conditions, the HER involves two elementary reaction steps. The first step is the Volmer step in which intermediate hydrogen adsorption ($H^+ + e^- + * = H^*$) occurs, and the second step is that molecular hydrogen is generated and leaves the catalyst site through Heyrovsky step ($H^* + H^+ + e^- = H_2 + *$) [36] or Tafel step ($2H^* = H_2 + 2*$). Thus, the overall HER can be described using the following equation under standard conditions:

$$H^+(\mathrm{aq}) + e^- \rightarrow \frac{1}{2}H_2(\mathrm{g}) \tag{1}$$

In this equation, an initial state $H^+(\mathrm{aq}) + e^-$, an intermediate adsorbed H*, and the final product $1/2H_2(\mathrm{g})$ are involved in the HER. The basic notion is that $\Delta G_H = 0$ is a necessary condition (but not sufficient) for a good catalyst [37, 38]. The HER performance for the transition metal atoms decorated on the $CuPS_3$ monolayer can be evaluated by computing the adsorption Gibbs free energy (ΔG_H) [39]. The value of ΔG_H for an ideal catalyst for HER should be close to zero [40] for the formation of

intermediate state H* and the easy release of H_2. ΔG_H can be calculated using the following equation:

$$\Delta G_H = \Delta E_H + \Delta E_{\mathrm{ZPE}} - T\Delta S_H \tag{2}$$

where ΔE_{ZPE} is the difference of zero-point energies between the adsorption state and the gas phase of H_2, and ΔS_H is the difference of entropy values between the adsorption state and the gas phase of H_2. At a temperature of 300 K and an atmospheric pressure of 1 bar, the value of $-T\Delta S_H$ of H_2 is calculated to be 0.20 eV [41]. ΔE_{H} can be calculated by the Eq. (3)

$$\Delta E_H = E_{*H} - E_* - \frac{1}{2}E_{H_2} - E_{\mathrm{BSSE}} \tag{3}$$

where E_{*H} and E_* are the total energies of $CuPS_3$ monolayer with and without hydrogen adsorption, respectively. E_{H_2} is the total energy of hydrogen molecule in the gas phase [40]. E_{BSSE} is the basis set superposition error (BSSE) caused by the artificial shortening of distances and enhanced interactions, which can be corrected by applying the counterpoise corrections using "ghost" atoms [42, 43].

Results and Discussion

Figure 1(a) shows the top view and side view of the pristine $CuPS_3$ monolayer. The Cu atoms are located in the middle of the monolayer and arranges in a hexagonal lattice. The P_2 dimers are located at the hexagonal center of Cu honeycomb lattice and are above and below the Cu plane. The Cu atoms and P_2 dimers are surrounded by six S atoms forming an octahedral complex. After the structural optimization using the DFT calculations, the lattice parameter of $CuPS_3$ monolayer is found to be $a = b = 5.90$ Å, and the (P-P) distance between the phosphorous atoms is 2.22 Å. The (Cu-Cu) distance between copper atoms is 3.39 Å, and the (P-S) distance between a phosphorous atom and a sulfur atom is 2.07 Å. All these results are consistent with those reported by Chittari et al. [29].

For monolayers of different ternary metal phosphosulfide compounds, the S^{2-} ions of the plane structure remain the constant, but the P-P distances are elongated in order to accommodate the metal atoms. The P-P distance in the $CuPS_3$ monolayer is slightly larger than that in $NiPS_3$ (2.15 Å) and equal to that in $CdPS_3$ (2.22 Å) [44]. Figure 1(b) shows the band structure of the optimized $CuPS_3$ monolayer, indicating that the $CuPS_3$ monolayer is a semiconductor material. The direct bandgap of $CuPS_3$ monolayer is 1.63 eV, and the conduction band minimum (CBM) and the valence band maximum (VBM) are located at the *K* point, which is in agreement with the previously reported theoretical calculated value of 1.76 eV [29]. Meanwhile, the plot of its projected density of states (PDOS) reveals its conductor characteristics. The PDOS results show that the energy splitting between the spin-up and spin-down occurs near the Fermi energy level, which is about 0.12 eV. The orbital of S 3p contributes most of the total density of states in the Fermi energy level. The metallic characteristic of $CuPS_3$ monolayer facilitates the transportation of electrons, which is beneficial for HER process [6].

Figure 2(a) shows possible positions for the adsorption of transition metal atoms on $CuPS_3$ monolayer, including the top of the copper atom (Cu), the top of the phosphorous atom (P), and the top of the S atom (S). The other possible sites were also tested, but they were all relaxed to one of the above three sites. The binding energy was calculated using the Eq. (5) to evaluate the stability of transition metal atoms adsorbed on the $CuPS_3$ monolayer,

$$E_{\mathrm{ads}} = E_{\mathrm{adatom}} + E_{\mathrm{CuPS_3}} - E_{\mathrm{adatom@CuPS_3}} \tag{5}$$

where E_{adatom} is the energy of a transition metal atom, $E_{\mathrm{CuPS_3}}$ is the total energy of pristine $CuPS_3$ monolayer after optimization, and $E_{\mathrm{adatom@CuPS_3}}$ is the total energy of the transition metal atom adsorption system. According to Eq. (5), the more positive the binding energy is, the better the adsorption of transition metal atoms on the $CuPS_3$ monolayer will be. The larger the binding energy is, the more stable the

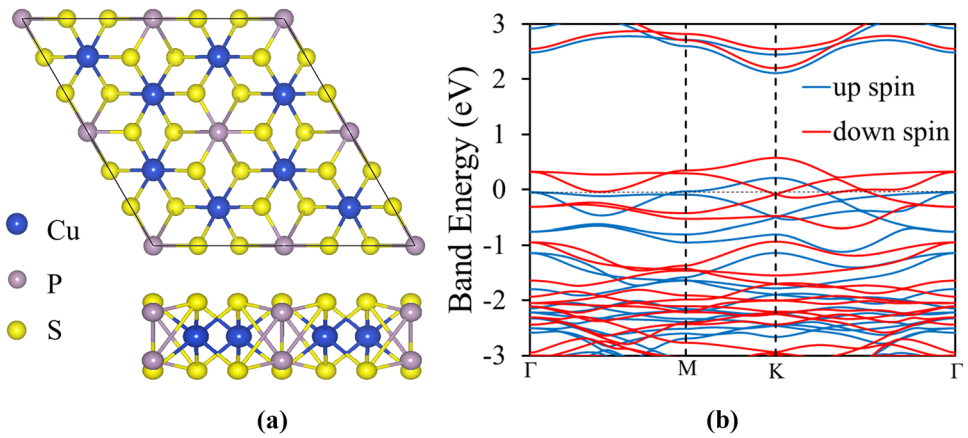

Fig. 1 (**a**) Top and side views of pristine $CuPS_3$ monolayer. (**b**) The calculated band structure of pristine $CuPS_3$ monolayer

transition metal atom adsorption system, which was also reported by Lin and Ni [45]. The calculated binding energies of the transition metal atom adsorption systems after their full optimizations are listed in Table 1. The calculated results showed that the Cu site is the optimum energy adsorption site for all the studied transition metal atoms. The binding energies are 8.98, 10.34, 11.32, 12.50, 13.20, 11.39, 10.89, and 8.71 eV for the systems based on Sc, Ti, V, Cr, Mn, Fe, Co, and Ni atoms, respectively. The strong binding of transition metal atoms and the 2D layer is beneficial for various physical and chemical applications.

The PDOS results of pristine and transition metal atoms decorated $CuPS_3$ monolayer are shown in Fig. 3. The electronic structure of the $CuPS_3$ monolayer near the Fermi level has apparently been changed by the adsorbed transition metal atoms.

For the Sc atoms adsorbed on the $CuPS_3$ monolayer (Fig. 3(b)), the peak of spin-up and spin-down Sc 3d states appears at about 1.49 eV, which is higher than the Fermi energy level. Meanwhile, the electronic states of P 3p and Cu 4 s remain similar values compared with that of the pristine $CuPS_3$ except the monolayer's Fermi energy level is shifted up about 0.32 eV, which is due to the charge transfer from Sc to S atoms in the $CuPS_3$ monolayer.

For the Ti atom adsorbed on the Cu site of the CuPS3 monolayer (Fig. 3(c)), the Fermi energy level is also shifted up by about 0.32 eV compared with that of the pristine CuPS3 monolayer. There are two peaks of the spin-up and spin-down total states, contributed by the Ti 3d states, and they are located at 1.85 eV and 1.99 eV above Fermi energy E_F, respectively.

For the V atom adsorbed at the Cu site of the $CuPS_3$ monolayer (Fig. 3(d)), the hybridization between the spin-up V 3d states and the S 3p states occurs near and below E_F. There exist two strong interactions between the spin-up V 3d states and the S 3p states, which occur at 0.78 eV and 1.86 eV, respectively. There are also three spin-down DOS peaks due to the hybridization between the V 3d states and the S 3p states, all above E_F. The electron states of V atom 3d orbital near E_F can effectively improve the electron domination and optimize the HER catalytic activity.

For the Cr atoms adsorbed on the $CuPS_3$ monolayer, they are strongly bound within the plane of this monolayer. Four main DOS peaks due to the hybridization of Cr 3d states and S 3p states are located below and around E_F for the spin-up state, as shown in Fig. 3(e). Two main spin-up Cr 3d peaks are located above E_F. At the same time, the Fermi energy level is shifted up by 0.25 eV.

For the Mn atom adsorbed on the $CuPS_3$ monolayer, there is a strong hybridization of spin-up Mn 3d states and S 3p states, which is located at 4.54 eV below the Fermi energy level as shown in Fig. 3(f). The spin-down Mn 3d peak appears above E_F in the range of 2.20 to 3.98 eV. The interaction is much weaker for the spin-down state than that for the spin-up state.

As shown in Fig. 3(g) and (h), there are two spin-up and spin-down DOS peaks for the Fe and Co atoms on the $CuPS_3$ monolayer. Among them, the spin-up peaks are contributed by the strong hybridization between the transition metal atom 3d states and S 3p states. The peak of Fe 3d orbital near E_F accelerates electron transfer during the catalytic process, which is beneficial to HER catalysis.

For the Ni atoms adsorbed on the $CuPS_3$ monolayer, there is an energy range from −4.81 to 0.98 eV for the hybridization of the Ni 3d states and S 3p states in Fig. 3(i). The 3d orbital of Ni atom is hybridized with the 3p orbital of P atom, and thus the Ni atoms are effectively adsorbed on the surface of $CuPS_3$ monolayer. In addition, Ni 3d orbit has a large peak near the Fermi energy level, which is beneficial for the electron transport in the catalytic process and thus the HER catalytic performance.

The catalytic performances of $CuPS_3$ monolayer decorated with the transition metal atom as the catalysts for HER were further evaluated by comparing their Gibbs adsorption free energies. In this study, a 2×2 supercell of pristine $CuPS_3$ was employed to model the basal plane. The

Table 1 Calculated binding energies (eV) for transition metal atoms adsorption system, and the catalytic active sites for HER with the Gibbs free energies for hydrogen adsorption

	Binding energies (eV)				HER				
	Cu	P	S	Optimum site	Adsorption site	ΔG_H (eV)	ΔG_{2H} (eV)	ΔG_{4H} (eV)	ΔG_{6H} (eV)
Sc	8.98	5.73	8.97	Cu	S_3	0.21	-	-	-
Ti	10.34	7.11	10.34	Cu	S_1	0.28	-	-	-
V	11.32	8.89	9.88	Cu	S_3	0.02	0.03	0.05	-0.10
Cr	12.50	10.35	10.35	Cu	S_3	0.18	-	-	-
Mn	13.20	10.78	12.01	Cu	S_3	0.35	-	-	-
Fe	11.39	9.11	10.29	Cu	S_3	0.11	0.47	1.23	1.53
Co	10.89	7.96	9.41	Cu	S_3	0.18	-	-	-
Ni	8.71	6.42	7.61	Cu	S_3	0.09	1.60	1.18	1.25
Pristine	-	-	-	-	-	0.44	-	-	-

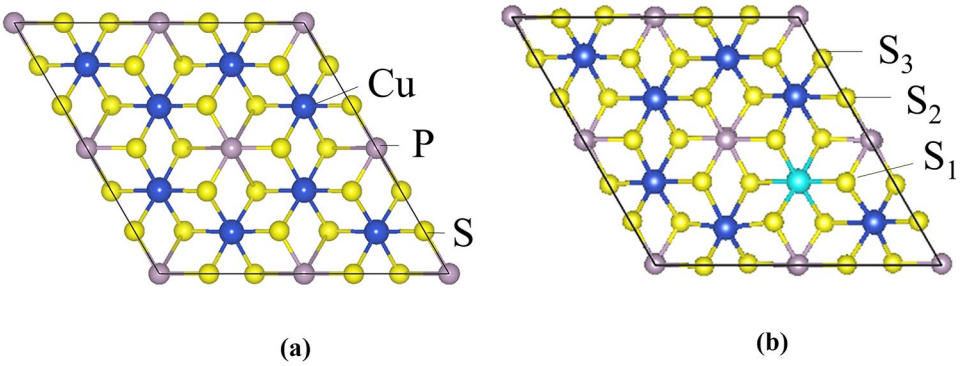

Fig. 2 (**a**) The possible adsorption sites of transition metal atoms in the $CuPS_3$ monolayer. (**b**) The possible adsorption positions of H atom on the transition metal atoms adsorption system

calculation results show that the top of the S atom is more energetically favorable for the H adsorption. The ΔG_H is 0.44 eV for the H atom absorbed onto the pristine $CuPS_3$ monolayer. Therefore, the H atom is difficult to be bound to the $CuPS_3$ monolayer because of its higher Gibbs free energy, which indicates that the pristine $CuPS_3$ monolayer has a poor catalytic performance for HER. For the transition metal atoms adsorbed onto the $CuPS_3$ monolayer system, there are three possible adsorption sites for H atoms, i.e., on the top of the S atom (S_1, S_2, and S_3) with different distances to the transition metal atom as shown in Fig. 2(b).

The Gibbs free energy values calculated by the density functional theory and the optimal adsorption sites of H atom on the transition metal atom system are listed in Table 1. The adsorption Gibbs free energy diagrams of HER on the pristine $CuPS_3$ pristine monolayer and transition metal decorated ones are shown in Fig. 4(a). The obtained values of ΔG_H for Sc, Ti, V, Cr, Mn, Fe, Co, and Ni adsorbed on the $CuPS_3$ monolayer are 0.21, 0.28, 0.02, 0.18, 0.35, 0.11, 0.18, and 0.09 eV, respectively. Among all the transition metal atoms, the ΔG_H values of V, Fe, and Ni atoms decorated $CuPS_3$ monolayer on the active site of S_3 are close to zero, indicating that the V, Fe, and Ni decorated $CuPS_3$ monolayers show good catalytic activities for the HER. Compared with the above results, the active site of the previously reported Ni adsorbed on $FePS_3$ monolayer at S_1

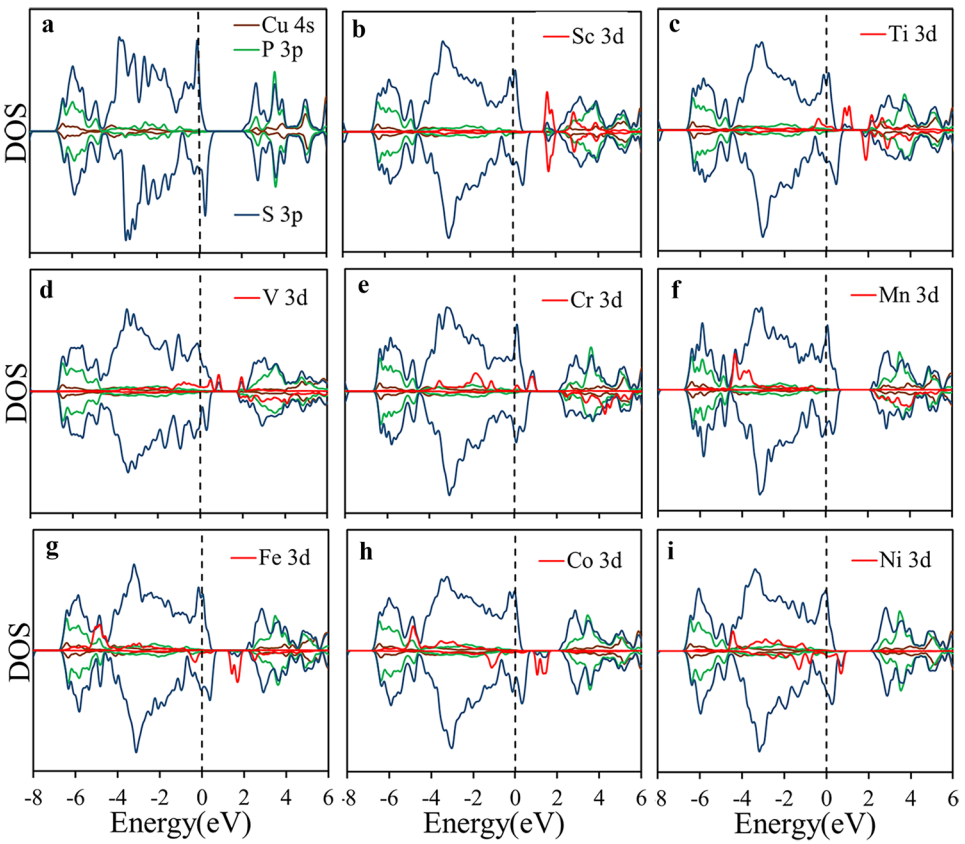

Fig. 3 Projected density of states (PDOS) plots for pristine CuPS3 (**a**), Sc (**b**), Ti (**c**), V (**d**), Cr (**e**), Mn (**f**), Fe (**g**), Co (**h**), and Ni (**i**) on CuPS3 monolayer at Cu site. The up-and-down plots present the spin-up and spin-down states, respectively

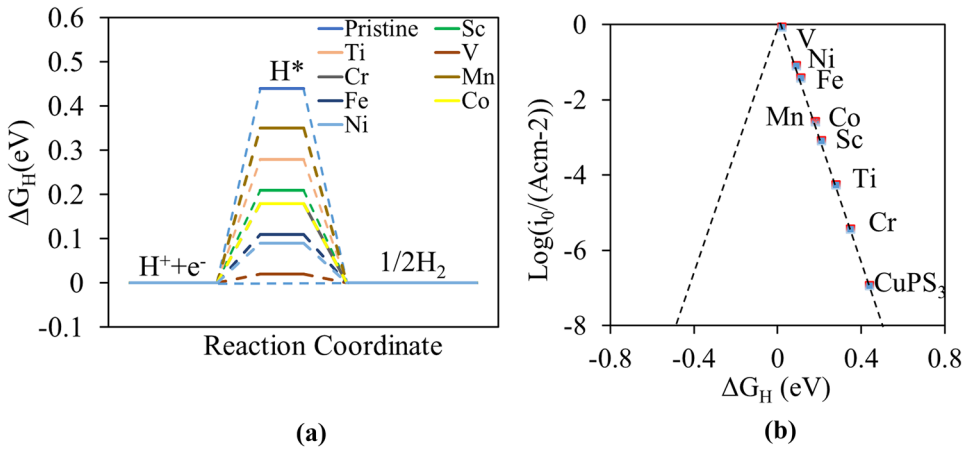

Fig. 4 (**a**) The adsorption Gibbs free energy diagram of HER at the equilibrium potential transition metal atoms anchored on the $CuPS_3$ monolayer. (**b**) The volcano curve of exchange current as a function of the adsorption Gibbs free energy

site is different with the Ni adsorbed on $CuPS_3$ monolayer, and the Gibbs free energy is 0.20 eV [28]. Theoretically Ni adsorbed on $CuPS_3$ monolayer has potentially higher HER catalytic activity than on $FePS_3$ monolayer. It was reported that the states around Fermi energy level is conducive to the adsorption of H, which will increase the catalytic activity of the material [46]. Form the above results, the 3d states peaks of V and Ni atoms are closer to the Fermi energy level than those of the other atoms; therefore, the V, Fe, and Ni decorated systems have potentially better catalytic performance than the other transition metal atoms for HER.

Based on Norskov's hypothesis [47], the catalytic performance of a catalyst for HER can be analyzed. The theoretical exchange current i_0 was calculated using the average Gibbs free energy of hydrogen adsorption on the catalyst [42]. The value of i_0 can be calculated using Eqs. (6) and (7) for $\Delta G_H > 0$ and $\Delta G_H < 0$, respectively, at pH = 0,

$$i_0 = -ek_0 \frac{1}{1 + \exp(\Delta G_H / k_b T)} \tag{6}$$

$$i_0 = -ek_0 \frac{1}{1 + \exp(-\Delta G_H / k_b T)} \tag{7}$$

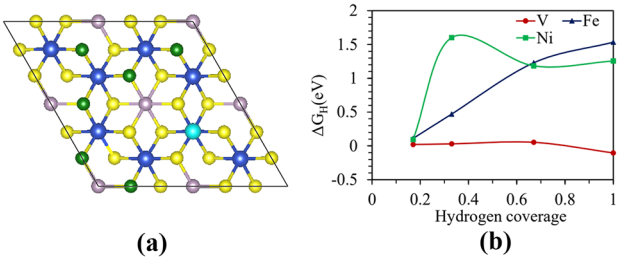

Fig. 5 (**a**) The catalytic active sites of H atom on the Fe Ni and V adsorbed on CuPS3 monolayer. The green atom is H atom. (**b**) The Gibbs free energy of H atom adsorption on the Fe Ni and V adsorbed on CuPS3 monolayer as function of hydrogen coverage

where k_0 is the reaction rate constant at zero overpotential, k_b is the Boltzmann constant, and T is the temperature. The obtained diagrams are plotted in Fig. 4(b). In this figure, the positions of i_0 and the values of ΔG_H for the catalysts reveal their catalytic performance for HER. The left side of the volcano curve shows the negative values of ΔG_H and the right side is corresponding to positive values of ΔG_H. The value of ΔG_H is zero at the top of the peak, which means that the closer to the top of the peak position, the better the HER performance of the catalyst [48]. As shown in Fig. 4(b), the ΔG_H values for the V, Fe, and Ni atom decorated $CuPS_3$ monolayer are located very close to the position of the volcano peak, indicating that these atoms anchored $CuPS_3$ monolayers are potentially good catalysts for HER. The rest of transition metal atoms adsorption system are located on the right of the curve as shown in Fig. 4(b), which are all far away from the position of the peak, indicating that the hydrogen atoms are difficult to be adsorbed onto the catalysts and they have weak catalytic effects on HER.

The effect the adsorption free energy of hydrogen coverage of H atom adsorption on electrocatalyst were further investigated. The hydrogen coverage ratio (θ_H) is defined as the ratio between the number of adsorbed H atoms (n) and the number of catalytic active sites (m), $\theta_H = n/m$. The catalytic active sites of H atom on the catalyst surface are shown in Fig. 5(a), and the Gibbs free energies for different hydrogen coverage ratio are shown in Fig. 5(b). The Gibbs free energies of hydrogen coverage for V, Fe, and Ni are listed in Table 1. For Fe and Ni adsorbed on $CuPS_3$ monolayer, the Gibbs free energy increases with the increase of hydrogen atomic coverage, indicating that Fe and Ni adsorbed on $CuPS_3$ monolayer are inert for HER for a large range of hydrogen coverage. However, for the V adsorbed on $CuPS_3$ monolayer, the Gibbs free energies for H atom adsorption are in the range from −0.10 to 0.02 eV for different hydrogen coverage ratios. The results prove that V adsorbed on $CuPS_3$ monolayer is catalytic active for HER for a large range of hydrogen coverage.

Conclusion

In brief, in this paper, electronic properties and the catalytic performance of HER for the $CuPS_3$ monolayer decorated by transition metal atoms were studied using the DFT calculation. Results show that all the transition metal atoms are closely bound to the Cu sites with a high binding energy. The pristine $CuPS_3$ monolayer has a poor catalytic performance for HER, and anchoring of transition metal atoms onto it can improve the catalytic performance of $CuPS_3$ monolayer. Among all these transition metal atoms, the values of ΔG_H for the systems of V, Fe, and Ni atoms are 0.02, 0.11, and 0.09 eV, respectively, which indicate the significantly improved catalytic performance of HER of $CuPS_3$ monolayer. At the same time, the influence of hydrogen coverage rate was calculated. The result shows that V adsorbed on $CuPS_3$ monolayer is catalytic active for HER for a large range of hydrogen coverage. This work provides a fundamental design methodology on how to improve the catalytic activity of catalysts based on monolayers of ternary metal phosphorus sulfide compounds.

Funding This work was financially supported by International Exchange Grant (IEC/NSFC/201078) through Royal Society UK and the National Natural Science Foundation of China (NSFC) NFSC.

Declarations

Conflict of Interest The authors declare no competing interests.

References

1. X. Long, G.X. Li, Z.L. Wang, H.Y. Zhu, T. Zhang, S. Xiao, W.Y. Guo, S.H. Yang, Metallic iron-nickel sulfide ultrathin nanosheets as a highly active electrocatalyst for hydrogen evolution reaction in acidic media. J. Am. Chem. Soc. **137**(37), 11900–11903 (2015)
2. H.H. Wu, H. Huang, J. Zhong, S. Yu, Q.B. Zhang, X.C. Zeng, Monolayer triphosphates MP3 (M = Sn, Ge) with excellent basal catalytic activity for hydrogen evolution reaction. Nanoscale **11**(25), 12210–12219 (2019)
3. L. Schlapbach, TECHNOLOGY Hydrogen-fuelled vehicles. Nature **460**(7257), 809–811 (2009)
4. E. Skulason, V. Tripkovic, M.E. Bjorketun, S. Gudmundsdottir, G. Karlberg, J. Rossmeisl, T. Bligaard, H. Jonsson, J.K. Norskov, Modeling the electrochemical hydrogen oxidation and evolution reactions on the basis of density functional theory calculations. J. Phys. Chem. C **114**(50), 22374–22374 (2010)
5. J.R. McKone, B.F. Sadtler, C.A. Werlang, N.S. Lewis, H.B. Gray, Ni-Mo nanopowders for efficient electrochemical hydrogen evolution. Acs. Catal. **3**(2), 166–169 (2013)
6. Q. Ding, B. Song, P. Xu, S. Jin, Efficient electrocatalytic and photoelectrochemical hydrogen generation using MoS2 and related compounds. Chem-Us **1**(5), 699–726 (2016)
7. C. Wan, Y.N. Regmi, B.M. Leonard, Multiple phases of molybdenum carbide as electrocatalysts for the hydrogen evolution reaction. Angew. Chem. Int. Edit. **53**(25), 6407–6410 (2014)
8. J.F. Xie, S. Li, X.D. Zhang, J.J. Zhang, R.X. Wang, H. Zhang, B.C. Pan, Y. Xie, Atomically-thin molybdenum nitride nanosheets with exposed active surface sites for efficient hydrogen evolution. Chem. Sci. **5**(12), 4615–4620 (2014)
9. J. Kibsgaard, T.F. Jaramillo, Molybdenum phosphosulfide: an active, acid-stable, earth-abundant catalyst for the hydrogen evolution reaction. Angew. Chem. Int. Edit. **53**(52), 14433–14437 (2014)
10. Q.Q. Zhang, J.Q. Guan, Single-atom catalysts for electrocatalytic applications. Adv. Funct. Mater. **30**(31), 2000768 (2020)
11. M.B. Gawande, P. Fornasiero, R. Zboril, Carbon-based single-atom catalysts for advanced applications. Acs. Catal. **10**(3), 2231–2259 (2020)
12. Y.J. Chen, S.F. Ji, C. Chen, Q. Peng, D.S. Wang, Y.D. Li, Single-atom catalysts: synthetic strategies and electrochemical applications. Joule **2**(7), 1242–1264 (2018)
13. L.C. Liu, A. Corma, Metal catalysts for heterogeneous catalysis: from single atoms to nanoclusters and nanoparticles. Chem. Rev. **118**(10), 4981–5079 (2018)
14. J. Wang, W.H. Fang, Y. Hu, Y.H. Zhang, J.Q. Dang, Y. Wu, B.Z. Chen, H. Zhao, Z.X. Li, Single atom Ru doping 2H-MoS2 as highly efficient hydrogen evolution reaction electrocatalyst in a wide pH range. Appl. Catal. B-Environ. **298**, 120490 (2021)
15. R. Gusmeao, Z. Sofer, M. Pumera, Exfoliated layered manganese trichalcogenide phosphite (MnPX3, X = S, Se) as electrocatalytic van der Waals materials for hydrogen evolution. Adv. Funct. Mater. **29**(2), 1805975 (2019)
16. C.Z. Zhu, Q.R. Shi, S. Feng, D. Du, Y.H. Lin, Single-atom catalysts for electrochemical water splitting. Acs. Energy. Lett. **3**(7), 1713–1721 (2018)
17. Y.R. Xue, B.L. Huang, Y.P. Yi, Y. Guo, Z.C. Zuo, Y.J. Li, Z.Y. Jia, H.B. Liu, Y.L. Li, Anchoring zero valence single atoms of nickel and iron on graphdiyne for hydrogen evolution. Nat. Commun. **9**, 1460 (2018)
18. Y.X. Sun, A.J. Huang, Z.G. Wang, Transition metal atom (Ti, V, Mn, Fe, and Co) anchored silicene for hydrogen evolution reaction. RSC Adv. **9**(45), 26321–26326 (2019)
19. Y.X. Chen, K.N. Yang, B. Jiang, J.X. Li, M.Q. Zeng, L. Fu, Emerging two-dimensional nanomaterials for electrochemical hydrogen evolution. J. Mater. Chem. A **5**(18), 8187–8208 (2017)
20. L. Chang, Z.X. Sun, Y.H. Hu, 1T Phase transition metal dichalcogenides for hydrogen evolution reaction. Electrochem. Energy R. **4**(2), 194–218 (2021)
21. H.L. Fei, J.C. Dong, D.L. Chen, J. Tour, Atomic cobalt on nitrogen-doped graphene for hydrogen generation. Nat. Commun. **6**, 8668 (2015)
22. H.J. Qiu, Y. Ito, W.T. Cong, Y.W. Tan, P. Liu, A. Hirata, T. Fujita, Z. Tang, M.W. Chen, Nanoporous graphene with single-atom nickel dopants: an efficient and stable catalyst for electrochemical hydrogen production. Angew. Chem. Inter. Edit. **54**(47), 14031–14035 (2015)

23. H.M. Wu, C.Q. Feng, L. Zhang, J.J. Zhang, D.P. Wilkinson, Non-noble metal electrocatalysts for the hydrogen evolution reaction in water electrolysis. Electrochem. Energy R. **4**(3), 473–507 (2021)
24. W.X. Chen, J.J. Pei, C.T. He, J.W. Wan, H.L. Ren, Y.Q. Zhu, Y. Wang, J.C. Dong, S.B. Tian, W.C. Cheong, S.Q. Lu, L.R. Zheng, X.S. Zheng, W.S. Yan, Z.B. Zhuang, C. Chen, Q. Peng, D.S. Wang, Y.D. Li, Rational design of single molybdenum atoms anchored on N-doped carbon for effective hydrogen evolution reaction. Angew. Chem. Int. Edit. **56**(50), 16086–16090 (2017)
25. W.Z. Li, M.Y. Liu, L. Gong, M.L. Zhang, C. Cao, Y. He, The electronic properties and catalytic activity of precious-metals adsorbed silicene for hydrogen evolution reaction and oxygen evolution reaction. Appl. Surf. Sci. **560**, 150041 (2021)
26. S.C. Yan, Z.S. Li, Z.G. Zou, Photodegradation of rhodamine B and methyl orange over boron-doped g-C3N4 under visible light irradiation. Langmuir **26**(6), 3894–3901 (2010)
27. Q. Pei, Y. Song, X.C. Wang, J.J. Zou, W.B. Mi, Superior electronic structure in two-dimensional MnPSe3/MoS2 van der Waals heterostructures. Sci. Rep. **7**, 9504 (2017)
28. C.Y. Tang, D. He, N. Zhang, X.Y. Song, S.F. Jia, Z.J. Ke, J.C. Liu, J.B. Wang, C.Z. Jiang, Z.Y. Wang, X.Q. Huang, X.H. Xiao, Electronic coupling of single atom and FePS3 boosts water electrolysis. Energy Environ. Mater. **0**, 1–7 (2021)
29. B.L. Chittari, Y. Park, D. Lee, M. Han, A.H. MacDonald, E. Hwang, J. Jung, Electronic and magnetic properties of single-layer MPX3 metal phosphorous trichalcogenides. Phys. Rev. B **94**(18), 184428 (2016)
30. H.J. Huang, J.N. Song, D.S. Yu, Y.A. Hao, Y.H. Wang, S.J. Peng, Few-layer FePS3 decorated with thin MoS2 nanosheets for efficient hydrogen evolution reaction in alkaline and acidic media. Appl. Surf. Sci. **525**, 146623 (2020)
31. A.R. Wildes, V. Simonet, E. Ressouche, G.J. McIntyre, M. Avdeev, E. Suard, S.A.J. Kimber, D. Lancon, G. Pepe, B. Moubaraki, T.J. Hicks, Magnetic structure of the quasi-two-dimensional antiferromagnet NiPS3. Phys. Rev. B **92**(22), 224408 (2015)
32. Y. Wang, J. Mao, X.G. Meng, L. Yu, D.H. Deng, X.H. Bao, Catalysis with two-dimensional materials confining single atoms: concept, design, and applications. Chem. Rev. **119**(3), 1806–1854 (2019)
33. M.S. José, A. Emilio, D.G. Julian, G. Alberto, J. Javier, O. Pablo, S.-P. Daniel, The SIESTA method for ab initio order- N materials simulation. J. Phys. Condens. Matter **14**(11), 2745 (2002)
34. J.P. Perdew, K. Burke, M. Ernzerhof, Generalized gradient approximation made simple. Phys. Rev. Lett. **77**(18), 3865–3868 (1996)
35. J.P. Perdew, K. Burke, M. Ernzerhof, Generalized gradient approximation made simple (vol 77, pg 3865, 1996). Phys. Rev. Lett. **78**(7), 1396–1396 (1997)
36. E. Skulason, G.S. Karlberg, J. Rossmeisl, T. Bligaard, J. Greeley, H. Jonsson, J.K. Norskov, Density functional theory calculations for the hydrogen evolution reaction in an electrochemical double layer on the Pt(111) electrode. Phys. Chem. Chem. Phys. **9**(25), 3241–3250 (2007)
37. P. Quaino, F. Juarez, E. Santos, W. Schmickler, Volcano plots in hydrogen electrocatalysis - uses and abuses. Beilstein J. Nanotech. **5**, 846–854 (2014)
38. W. Schmickler, S. Trasatti, Comment on "Trends in the exchange current for hydrogen evolution." Electrochem. Soc. 152, J23 (2005). J. Electrochem. Soc. **153**(12), L31-L32 (2006)
39. J.K. Norskov, J. Rossmeisl, A. Logadottir, L. Lindqvist, J.R. Kitchin, T. Bligaard, H. Jonsson, Origin of the overpotential for oxygen reduction at a fuel-cell cathode. J. Phys. Chem. B **108**(46), 17886–17892 (2004)
40. J. Bonde, P.G. Moses, T.F. Jaramillo, J.K. Norskov, I. Chorkendorff, Hydrogen evolution on nano-particulate transition metal sulfides. Faraday Discuss. **140**, 219–231 (2008)
41. D. Voiry, H. Yamaguchi, J.W. Li, R. Silva, D.C.B. Alves, T. Fujita, M.W. Chen, T. Asefa, V.B. Shenoy, G. Eda, M. Chhowalla, Enhanced catalytic activity in strained chemically exfoliated WS2 nanosheets for hydrogen evolution. Nat. Mater. **12**(9), 850–855 (2013)
42. I.G. Shuttleworth, Investigation of the H-Cu and Cu–Cu bonds in hydrogenated Cu. J. Phys. Chem. Solids **74**(1), 128–134 (2013)
43. I.G. Shuttleworth, Strategies for reducing basis set superposition error (BSSE) in O/AU and O/Ni. J. Phys. Chem. Solids **86**, 19–26 (2015)
44. F.M. Wang, T.A. Shifa, P. Yu, P. He, Y. Liu, F. Wang, Z.X. Wang, X.Y. Zhan, X.D. Lou, F. Xia, J. He, New frontiers on van der Waals layered metal phosphorous trichalcogenides. Adv. Funct. Mater. **28**(37), 1802151 (2018)
45. X.Q. Lin, J. Ni, Much stronger binding of metal adatoms to silicene than to graphene: a first-principles study. Phys. Rev. B **86**(7), 075440 (2012)
46. J.K. Norskov, F. Abild-Pedersen, F. Studt, T. Bligaard, Density functional theory in surface chemistry and catalysis. P. Natl. Acad. Sci. USA **108**(3), 937–943 (2011)
47. A. Jain, Y. Shin, K.A. Persson, Computational predictions of energy materials using density functional theory. Nat. Rev. Mater. **1**, 15004 (2016)
48. Y.A. Zhou, G.P. Gao, Y. Li, W. Chu, L.W. Wang, Transition-metal single atoms in nitrogen-doped graphenes as efficient active centers for water splitting: a theoretical study. Phys. Chem. Chem. Phys. **21**(6), 3024–3032 (2019)